JOURNAL OF THERMOPHYSICS AND HEAT TRANSFER
Vol. 9, No. 4, October–December 1995

Nonequilibrium Boundary-Layer Effects on the Aerodynamic Heating of Hypersonic Waverider Vehicles

George R. Inger*
Iowa State University, Ames, Iowa 50011-3231

The aerodynamic heating of hypersonic waverider vehicle configurations is examined in the high-altitude hypersonic flight regime where nonequilibrium dissociation–recombination in the boundary-layer and finite surface catalysis effects are both important. Analytical treatment of these effects is given for highly cooled surfaces in three important heating regions: 1) the nose, 2) the swept-wing leading-edge attachment line, and 3) the windward body centerline. Relationships for the relative nonequilibrium effects are developed for each region that enable both computer code-prediction validation and cost-effective parametric engineering studies.

Nomenclature

C_D = equilibrium constant, Eq. (8a)
$\hat{C}_p$ = specific heat of molecules
F^* = boundary-layer form factor, Eq. (31)
f = boundary-layer velocity similarity function, Eq. (2)
G = composition-dependent portion of reaction rate, Eq. (8)
g_z = $I_z(\eta)/I_z(\infty)$, Eq. (18)
h_D = specific dissociation energy of molecules
I_z, I_θ = boundary-layer profile integrals, Eq. (15)
K_w = speed of catalytic atom recombination on body surface
k_r' = recombination rate constant
Le = Lewis number, Pr/Sc
Pr = Prandtl number
p = static pressure
Q_w = nondimensional heat transfer rate, Eq. (10)
$\dot{q}_w$ = surface heat transfer rate per unit area
R_m = molecular gas constant
R_u = universal gas constant
$R_{x,z}$ = nose radii of curvature, Fig. 2
$\mathcal{R}$ = net reaction rate distribution function, $\theta^{\omega-2}G$, Eq. (8)
r = $(dw_e/dz)/(du_e/dx) = R_x/R_z$
Sc = Schmidt number
s = w/w_e
T = absolute temperature
U_∞ = freestream (flight) velocity
$\mathcal{U}$ = $U_\infty^2/2\hat{C}_pT_e$
u, w = chordwise, spanwise velocity components
x, y, z = coordinates in streamwise, normal, and spanwise directions
Z = $\alpha(0)/\alpha_F(0)$, Eq. (20)
α = atom mass fraction
β_s = inviscid flow stagnation point velocity gradient, $(du_e/dx)_s$
$\tilde{\Gamma}_c$ = $\Gamma_c/0.47Sc^{1/3}$
Γ_c = Dähmkohler number for surface reactions
Γ_D = Dähmkohler number for dissociation-dominated flow, Eq. (30)
Γ_G = Dähmkohler number for gas-phase recombination
Γ^* = composite Dähmkohler number for combined gas phase and surface reactions, Eq. (20)
γ = specific heat ratio
γ_c = catalytic efficiency of wall material
ΔQ = nonequilibrium heat transfer function, Eq. (32)
η, ξ = boundary-layer similarity coordinates
θ = T/T_e
θ_D = $h_D/(R_mT_e)$, characteristic nondimensional dissociation temperature
Λ = sweepback angle, Fig. 10
μ = coefficient of viscosity
ρ = mixture density
υ_D = dissociation rate integral, Eq. (31)
$\upsilon_{Z,\theta}$ = reaction rate integrals, Eq. (16)
ω = recombination rate temperature-dependence exponent, as in $k_r = k_r'T^\omega$

Subscripts
EQ = value for equilibrium boundary-layer flow
e = boundary-layer edge conditions
F = value for frozen boundary-layer flow
M = denotes molecule
s = inviscid flow conditions at stagnation point
w = conditions on body surface
0 = conditions at zero sweep
∞ = freestream conditions
$'$ = $\partial(\ )/\partial\eta$
$*$ = value at max temperature point in boundary layer

Received May 12, 1994; revision received March 7, 1995; accepted for publication March 31, 1995.

*Professor, Department of Aerospace Engineering and Engineering Mechanics. Associate Fellow AIAA.

Introduction

THE interest in aerodynamically efficient waverider vehicle configurations has led to recently proposed new applications to lifting atmospheric flight, orbital transfer, and planetary atmosphere entry.[1] In such applications, the question of high aerodynamic heating in certain areas of the configuration will be an important aspect of the design analysis,[2] as will high-temperature dissociation effects on this heating. Moreover, owing to the combination of high flight speeds (short flow residence times) and lower density high-altitude operating conditions (long chemical reaction collision times), such dissociation effects can involve marked departures from gas phase chemical equilibrium in the boundary layer and finite rates of catalytic atom recombination along the vehicle surface. These nonequilibrium effects in turn cause significant reductions in aerodynamic heating if the body surface is not fully catalytic.[3] Consequently, it is appropriate to address the

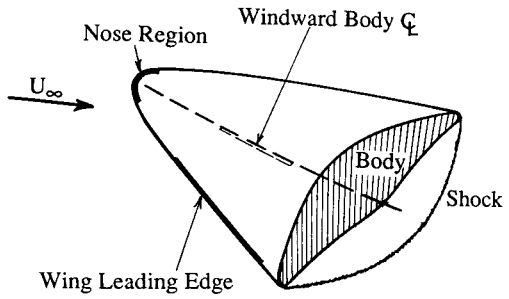

Fig. 1 Typical cone-derived waverider configuration and its regions of aerodynamic heating concern.

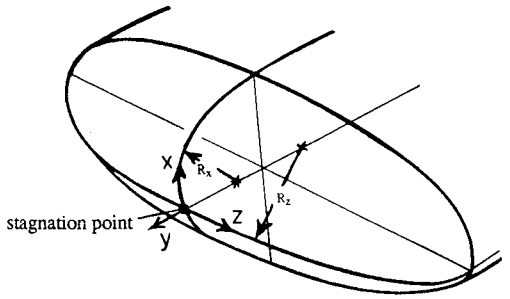

Fig. 2 Nose region: generalized three-dimensional stagnation flow.

issue of predicting the nonequilibrium heat transfer rates to key regions on the vehicle and how these depend on the catalytic properties of the surface material.

This article deals with this issue for a cone-derived waverider configuration that is fairly typical (see Fig. 1). The body is taken to be highly cooled ($T_w/T_s << 1$) and the boundary layer along it to be laminar and steady. We focus specifically on the three regions (nose, attachment line along the swept wing leading edge, and the windward body surface centerline, as delineated in Fig. 1), where the heat transfer aspect is of most interest, and then give a theoretical analysis of the nonequilibrium effects unique to each. We emphasize an approach here that is analytical rather than purely numerical, in order to provide results that can serve advanced engineering design analysis, illuminate the relative role of kinetic rates and surface catalysis, and provide a basis for computational fluid dynamics (CFD) code-result validation.

Assumptions and General Formulation

We consider airflow in the shock layer around a highly cooled body under such hypervelocity flight conditions that the postshock dissociative and vibrational chemistry can be taken as fully equilibrated upon reaching the boundary-layer edge. That is, we confine attention to that range of altitude/speed flight conditions where there is a distinct inviscid shock-layer region across which the dissociative relaxation time is very short compared to the reaction time within either the underlying boundary layer or upon the body surface. This boundary-layer regime, which pertains to flight altitudes below 200–250 k-ft (depending on body size), still contains a large amount of the interesting nonequilibrium dissociation effects on heating before the onset of dissociative nonequilibrium in the fully viscous shock-layer regime (see the NASA report by Chung[4] on this point, especially Fig. 6 therein).

The analysis may be further expedited without loss of the essential nonequilibrium flow thermophysics by introducing the following simplifying assumptions:

1) As far as heat transfer is concerned, the gas mixture can be adequately approximated by a binary mixture of atoms and molecules with equal specific heats and negligible thermal diffusion between them.

2) The Prandtl and Lewis numbers are near unity and, like the viscosity-density product, are constant across the boundary layer.

3) The chemical reaction effects on the boundary-layer velocity profile solutions (via the reciprocal density coefficient of the pressure gradient term in the momentum equations) are small enough for a highly cooled wall to permit taking these profiles as known distributions in the leading approximation.

4) Catalytic recombination of atoms on the body surface is governed by a first-order rate law with negligible heterogeneous dissociation.[3]

5) The freestream is strongly hypersonic, since the dissociation effects of interest here only occur at such flight speeds.

For such a flow model, a convenient description of the nonequilibrium-dissociated boundary-layer flowfield is obtained by introducing the Levy–Lees transformation[5]

$$\eta = (1 + r)\frac{u_e}{\sqrt{2\xi}}\int_0^y \rho\, dy \tag{1a}$$

$$\xi = \int_0^x \rho_w \mu_w u_e\, dx \tag{1b}$$

plus the following nondimensional chordwise x and spanwise z velocity and temperature variables (Fig. 2):

$$u/u_e = \frac{\partial f}{\partial \eta} \cong f'(\xi, \eta) \tag{2}$$

$$w/w_e = s(\xi, \eta) \tag{3}$$

$$T/T_e = \theta(\xi, \eta) \tag{4}$$

We then have the following equations governing the thermochemistry in the flow:

$$Scf\frac{\partial \alpha}{\partial \eta} + \frac{\partial^2 \alpha}{\partial \eta^2} - 2\xi\left(\frac{\partial \alpha}{\partial \xi}\frac{\partial f}{\partial \eta} - \frac{\partial f}{\partial \xi}\frac{\partial \alpha}{\partial \eta}\right) = \mathcal{R}(\alpha, \theta) \tag{5}$$

$$\theta \cong \theta_w + (1 - \theta_w)\cdot Pr^{1/3} f' + (\sqrt{Pr}/2C_p T_e)[u_e^2(f'\cdot Pr^{1/3} - f'^2) + w_e^2(f'\cdot Pr^{1/3} - s^2)] + (h_D/\hat{C}_p T_e)[(\alpha_e - \alpha_w)f'\cdot Sc^{1/3} + \alpha_w - \alpha] \tag{6}$$

where the latter equation is obtained from the generalized Crocco energy equation integral pertaining to highly cooled wall conditions,[6] and where from assumption 3, stated earlier, f' and s are regarded as known functions from appropriate solutions of the chordwise and spanwise momentum equations, respectively.[7]

The term $\mathcal{R}(\alpha, \theta)$ on the right side of atomic species conservation Eq. (5) is the nondimensional net gas-phase recombination rate; for a binary mixture of atoms and molecules undergoing the dissociation–recombination reaction

$$A_2 + X \underset{kr}{\overset{kd}{\rightleftarrows}} 2A + X \tag{7}$$

(where A_2, A, and X denote a molecule, atom, and any third body, respectively, and $k_r = k_r' T^{\omega}$ is the recombination rate), this function is

$$\mathcal{R} = \Gamma_G\cdot\theta^{\omega-2}\{[\alpha^2/(1 + \alpha)] - (C_D/p_e)(1 - \alpha)e^{-\theta_D/\theta}\} \equiv \Gamma_G\cdot G(\alpha, \theta) \tag{8a}$$

Here, C_D is an equilibrium constant and Γ_G is a characteristic local flow time/gas-phase reaction time ratio (Dähmkohler number) defined by

$$\Gamma_G \equiv \frac{4k_r' T_e^{\omega-2} p_e^2 \xi}{u_e R_u^2 \left(\frac{d\xi}{dx}\right)[1+r]} \tag{8b}$$

where $r = (dw_e/dz)/(du_e/dx)$ is the ratio of the spanwise to streamwise inviscid velocity gradients. The function $\theta^{\omega-2}$ in Eq. (8a) represents the temperature profile effect on the recombination rate and pre-exponential portion of the dissociation rate; since $\omega \cong -1.5$ for air, this effect has a considerable influence on the nonequilibrium behavior across a highly cooled boundary layer.[8] The function $G(\alpha, \theta)$ represents the composition-dependence of the reaction rate and involves a contribution from both the local recombination ($\sim\alpha^2$) and dissociation rates; it vanishes identically when the boundary layer is in equilibrium ($\Gamma_G \to \infty$), but does not in the opposite extreme of chemically frozen flow ($\Gamma_G \to 0$).

The boundary conditions at the edge of the boundary layer ($\eta \to \infty$) are that $s(\xi, \infty) = f'(\xi, \infty) = \theta(\xi, \infty) = 1$ along with the inviscid equilibrium–dissociation condition $G(\xi, \infty) = 0$, $\alpha = \alpha_e = \alpha_{EQ}(T_e)$, where $\alpha_e^2 = (1 - \alpha_e^2)C_D e^{-\theta_D/p_e}$. Along the arbitrarily catalytic cold impermeable wall surface, $\theta(\xi, 0) = \theta w << 1$ and $s(\xi, 0) = f(\xi, 0) = f'(\xi, 0) = 0$ for no velocity or thermal slip. Furthermore, there is the atomic species boundary condition

$$\frac{\partial\alpha}{\partial\eta}(\xi, 0) = \sqrt{\frac{2\rho_w \xi}{\mu_w u_e \left(\frac{d\xi}{dx}\right)[1+r]}}\, S_c K_w \cdot \alpha(\xi, 0) \equiv \Gamma_c \cdot \alpha_w \tag{9}$$

where Γ_c is the characteristic local diffusion time to recombination time ratio (or heterogeneous Dähmkohler number) expressed in terms of the atom recombination velocity K_w on the surface. The parameter K_w is a known function of the wall temperature and material[3] that is related to the surface catalytic efficiency γ_c by $\gamma_c \equiv (\pi K_w^2/R_m T_w)^{1/2}$. The boundary condition (9) expresses the fact that the rate of diffusion of atoms from the gas is balanced by the rate of catalytic recombination on the wall surface. When $\Gamma_c \to \infty$, the surface is completely catalytic [$\alpha(0) = 0$], whereas in the other extreme, $\Gamma_c = 0$, the surface is noncatalytic and the wall atom diffusion vanishes [$(\partial\alpha/\partial\eta)_w = 0$].

Once the foregoing split boundary value problem for $\alpha(\eta)$ is solved, the corresponding nondimensional wall heat transfer rate may be determined from

$$Q_w \equiv \frac{-P_R(\dot{q}_w/\hat{C}_p T_e)}{\sqrt{\rho_w \mu_w u_e \left[\left(\frac{d\xi}{dx}\right)\Big/ 2\xi\right][1+r]}} = \frac{\partial\theta}{\partial\eta}(\xi, 0) + \frac{Le h_D}{\hat{C}_p T_e} \cdot \frac{\partial\alpha}{\partial\eta}(\xi, 0) \tag{10}$$

Clearly, only heat conduction contributes to the heat transfer when the wall is completely noncatalytic [$\alpha'(0) = 0$].

Nose Region

In close-up view, this involves a stagnation type of flow with two unequal principal radii of body curvature R_x and R_z (see Fig. 2) such that $r = R_x/R_z$ (Ref. 7). The flow is a self-similar one ($\partial/\partial\xi = 0$) with $u_e = \beta_s x$ and both $u_e^2/\hat{C}_p T_e$ and $w_e^2/\hat{C}_p T_e$ vanishingly small in Eq. (6). Consequently, the nonequilibrium effects within the highly cooled boundary layer are dominated by gas-phase recombination regardless of the surface catalycity.[8] The highly cooled wall situation also admits a further simplification in that the spanwise velocity profile is then known to be well approximated by[7]

$$s(\eta) \cong f'(\eta) \tag{11}$$

thereby reducing our task to solving Eqs. (5) and (6) subject to the aforementioned boundary conditions.

It is of interest to note at this point the role of nose geometry in determining the finite rate chemistry effects. Regarding the gas phase, it can be seen from expression (8b) that increasing r reduces Γ_G, thereby promoting a tendency toward chemically frozen behavior; this is because a larger value of r implies a higher resultant flow velocity, and hence, a smaller flow residence time at a given x. Likewise, the catalytic surface reaction parameter Γ_c of Eq. (9) is also reduced by increasing r, reflecting the fact that a larger r reduces the thickness, and hence, the diffusion time across the boundary layer. Although r tends to be small compared to unity for waverider configurations, we retain an arbitrary value here for the sake of generality.

An accurate approximate solution for the surface properties under arbitrary nonequilibrium conditions for all values of r can now be obtained as follows. First, we perform a purely formal double integration of Eq. (5) with respect to η to obtain, after applying the boundary conditions and carrying out some algebra, the relations

$$\frac{\alpha(0)}{\alpha_F(0)} = \frac{\alpha'(0)}{\alpha_F'(0)} = 1 - \frac{\alpha_s \Gamma_G}{1+\alpha_s}\vartheta_z(\infty) \tag{12}$$

$$\theta'(0) = \frac{1 - \theta_w + [\alpha_s \Gamma_G h_D/(1+\alpha_s)]\vartheta_\theta(\infty)}{I_\theta(\infty)} = \left[\frac{1-\theta_w}{I_\theta(\infty)}\right] + \frac{h_D \vartheta_\theta(\infty)}{I_\theta(\infty)\vartheta_z(\infty)}\left[1 - \frac{\alpha(0)}{\alpha_F(0)}\right] \tag{13}$$

where

$$\alpha_F(0) = \frac{\alpha_F'(0)}{\Gamma_c} = [1 + \Gamma_c I_z(\infty)]^{-1}\alpha_s \tag{14}$$

$$I_z(\infty) \equiv \int_0^\infty \exp\left(-Sc\int_0^\infty f\, dn\right) \cong (0.47 S_c^{1/3})^{-1} \tag{15}$$

$$\vartheta_z(\infty) \equiv \int_0^\infty \exp\left(-Sc\int_0^\eta f\, d\eta\right) \times \left[\int_0^\eta \exp\left(Sc\int_0^\eta f\, d\eta\right)\mathcal{R}\, d\eta\right] d\eta \tag{16}$$

where I_θ and ϑ_θ are obtained from Eqs. (15) and (16), respectively, by replacing Sc by Pr in the exponentials. Here, α_F is the frozen flow solution for arbitrary surface catalycity,[3] and θ_F the corresponding temperature profile [obtained by dropping the last term proportional to h_D in Eq. (6)]. Second, we apply the fact that the ratio $\vartheta_\theta/\vartheta_z$ is a weak function of Le only, and the fact that the terms on the right side of Eq. (13) not involving $\alpha(0)$ are equal to $\theta'_{EQ}(0)$ for a highly cooled wall; Eqs. (12) and (13) consequently yield the following simple nondimensional ratios:

$$1 - \frac{\alpha(0)}{\alpha_F(0)} = 1 - \frac{\alpha'(0)}{\alpha_F'(0)} = \frac{\theta'(0) - \theta_F'(0)}{\theta'_{EQ}(0) - \theta_F'(0)} = \frac{Q_w - Q_{w,F}}{Q_{w,EQ} - Q_{w,F}} \tag{17}$$

regardless of the values of Sc, Pr, Γ_G, or Γ_c. Equation (17) indicates that solving the species conservation equation suffices to determine all the nonequilibrium conditions at the surface once the frozen and equilibrium values are known. Third, we take advantage of a very detailed study[8] of the net reaction rate function for highly cooled walls, which showed that the recombination-dominated nature of the chemistry leads to a convenient yet accurate approximation for $\mathcal{R}$ over the entire range of nonequilibrium behavior and surface catalycity; upon taking $C_D/p_e = \alpha_e^2 e^{\theta_D}/(1 - \alpha_e^2)$ from the outer boundary condition, this is

$$\mathcal{R} \cong \left[\frac{1 + \alpha_s}{1 + \alpha(0)}\right] \theta_F^{\omega-2} \left\{\alpha^2(0) + \frac{2\alpha(0)\alpha'(0)}{0.47Sc^{1/3}} g_z + \left[\frac{\alpha'(0) g_z}{0.47Sc^{1/3}}\right]^2\right\} \left\{1 - \exp\left[\frac{-\theta_D}{\theta_F}(1 - \theta_F)\right]\right\} \alpha_s^{-2} \tag{18a}$$

where

$$g_z(\eta) \equiv \left[\frac{I_z(\eta)}{I_z(\infty)}\right] \tag{18b}$$

The reaction rate integral (16) then takes the value

$$\vartheta_z(\infty) \cong \left[\frac{1 + \alpha_s}{1 + \alpha(0)}\right] \left\{\alpha^2(0)\vartheta_{z_{F,1}} + \frac{2\alpha(0)\alpha'(0)}{0.47Sc^{1/3}} \vartheta_{z_{F,2}} + \left[\frac{\alpha'(0)}{0.47Sc^{1/3}}\right]^2 \vartheta_{z_{F,3}}\right\} \alpha^{-2} \tag{19a}$$

where

$$\vartheta_{z_{F,1}} \equiv \int_0^\infty \exp\left(-Sc \int_0^\eta f\, d\eta\right) \left[\int_0^\eta \exp\left(Sc \int_0^\eta f\, d\eta\right) \times \theta_F^{\omega-2} \left\{1 - \exp\left(-\frac{\theta_D}{\theta_F}(1 - \theta_F)\right)\right\} d\eta\right] d\eta \tag{19b}$$

$$\vartheta_{z_{F,2}} \equiv \int_0^\infty \exp\left(-Sc \int_0^\eta f\, d\eta\right) \left[\int_0^\eta \exp\left(Sc \int_0^\eta f\, d\eta\right) \times \theta_F^{\omega-2} \left\{g_z(\eta) - \exp\left(-\frac{\theta_D}{\theta_F}(1 - \theta_F)\right)\right\} d\eta\right] d\eta \tag{19c}$$

$$\vartheta_{z_{F,3}} \equiv \int_0^\infty \exp\left(-Sc \int_0^\eta f\, d\eta\right) \left[\int_0^\eta \exp\left(Sc \int_0^\eta f\, d\eta\right) \times \theta_F^{\omega-2} \left\{g_z^2(\eta) - \exp\left(-\frac{\theta_D}{\theta_F}(1 - \theta_F)\right)\right\} d\eta\right] d\eta \tag{19d}$$

are known quadratures of the frozen-flow solution that have been evaluated and extensively tabulated[8] (typical values, which are insensitive to small variations in Sc and Pr, are presented here for convenience in Figs. 3a–3c). Equation (12) then yields a simple quadratic equation for the nonequilibrium atom concentration at the wall whose solution is

$$Z \equiv \frac{\alpha(0)}{\alpha_F(0)} = \frac{\sqrt{[1 + \alpha_F(0)]^2 + 4\Gamma^*} - [1 - \alpha_F(0)]}{2[\alpha_F(0) + \Gamma^*]} \tag{20a}$$

where in terms of $\tilde{\Gamma}_c \equiv \Gamma_c/0.47Sc^{1/3}$

$$\Gamma^* = \alpha_s \left[\frac{\vartheta_{z_{F,1}} + 2\tilde{\Gamma}_c \vartheta_{z_{F,2}} + \tilde{\Gamma}_c^2 \vartheta_{z_{F,3}}}{(1 + \tilde{\Gamma}_c)^2}\right] \Gamma_G \tag{20b}$$

is a composite Dähmkohler number representing the simultaneous effects of the finite gas-phase and surface reaction rates, as well as the influence of wall temperature and all the thermochemical properties of the gas. The corresponding nonequilibrium heat transfer is then obtained directly from Eq. (17), which involves the following equilibrium and frozen limits obtained by applying Eq. (10) in conjunction with appropriate values from Eqs. (12–14):

$$Q_{w,EQ} \approx 0.47P_R^{1/3}\left(1 - \theta_w + L_e^{0.52} \frac{\alpha_s h_D}{\hat{C}_p T_s}\right) \tag{21}$$

$$Q_{w,F} \approx 0.47P_R^{1/3}\left[1 - \theta_w + L_e^{0.67} \frac{\alpha_s h_D}{\hat{C}_p T_s}\left(\frac{\tilde{\Gamma}_c}{1 + \tilde{\Gamma}_c}\right)\right] \tag{22}$$

Equation (22), originally given by Goulard,[3] clearly indicates that low-to-moderate catalysis rates can significantly reduce heat transfer when the boundary layer is well out of gas phase equilibrium.

Equation (20a) is plotted vs Γ^* in Fig. 4, from which it is seen that it is very insensitive to the parameter $\alpha_F(0)$, and hence, essentially a universal function of Γ^* alone. Using the average value $\alpha_F(0) = \frac{1}{2}$, the relationships from Eq. (17) that

$$\frac{Q_w - Q_{w,F}}{Q_{w,EQ} - Q_{w,F}} \approx 1 - Z(\Gamma^*) \tag{23a}$$

$$\frac{\alpha(0)}{\alpha_F(0)} = Z(\Gamma^*) \cong \frac{3\sqrt{1 + (16\Gamma^*/9)} - 1}{2 + 4\Gamma^*} \tag{23b}$$

thus constitute a nonequilibrium similitude law for combined gas-phase/catalytic surface reaction effects in the recombination-dominated case. It should be noted that Eqs. (23) encompass the entire extent of these effects depending on the respective values of the two Dähmkohler number parameters Γ_G and Γ_c. For example, the limit $\Gamma_G >> 1$ corresponds to equilibrium–dissociation behavior throughout the boundary layer, giving $Z \to 0$, and hence, $q_w \to q_{w,EQ}$. The opposite limit $\Gamma_G \to 0$ pertains to a chemically frozen (nonreacting) boundary layer with $Z \to 1$, giving from Eq. (22) a heat transfer rate that is highly dependent on the degree of finite wall catalycity reflected in the prevailing value of Γ_c.

Predictions obtained from Eq. (23) are found to agree well with exact numerical solutions of the general stagnation boundary-layer equations over a wide range of both gas-phase nonequilibrium states (Γ_G) and surface catalycity effects (Γ_c). An example is shown in Fig. 5, where the good agreement (within 5–10%) with Fay and Riddell's well-known results[9] over the entire nonequilibrium dissociation–recombination boundary-layer regime is illustrated. A further application is illustrated in Fig. 6, where the nonequilibrium heat transfer vs altitude is shown for a typical case as a function of various assumed values of the wall catalytic efficiency. The resulting significant reduction in heating predicted by the present theory for moderately to weakly catalytic walls is seen to be in good agreement with Chung's[4] exact numerical solutions.

The closed form of the foregoing analysis not only provides valuable physical insight, but also a very efficient computational model of how various design parameters influence the relative nonequilibrium effect on heat transfer. In particular, it can be used as an interpolative relationship between any frozen and equilibrium heat transfer solution routines the user wishes to supply. In the present work we have used Eqs. (21)

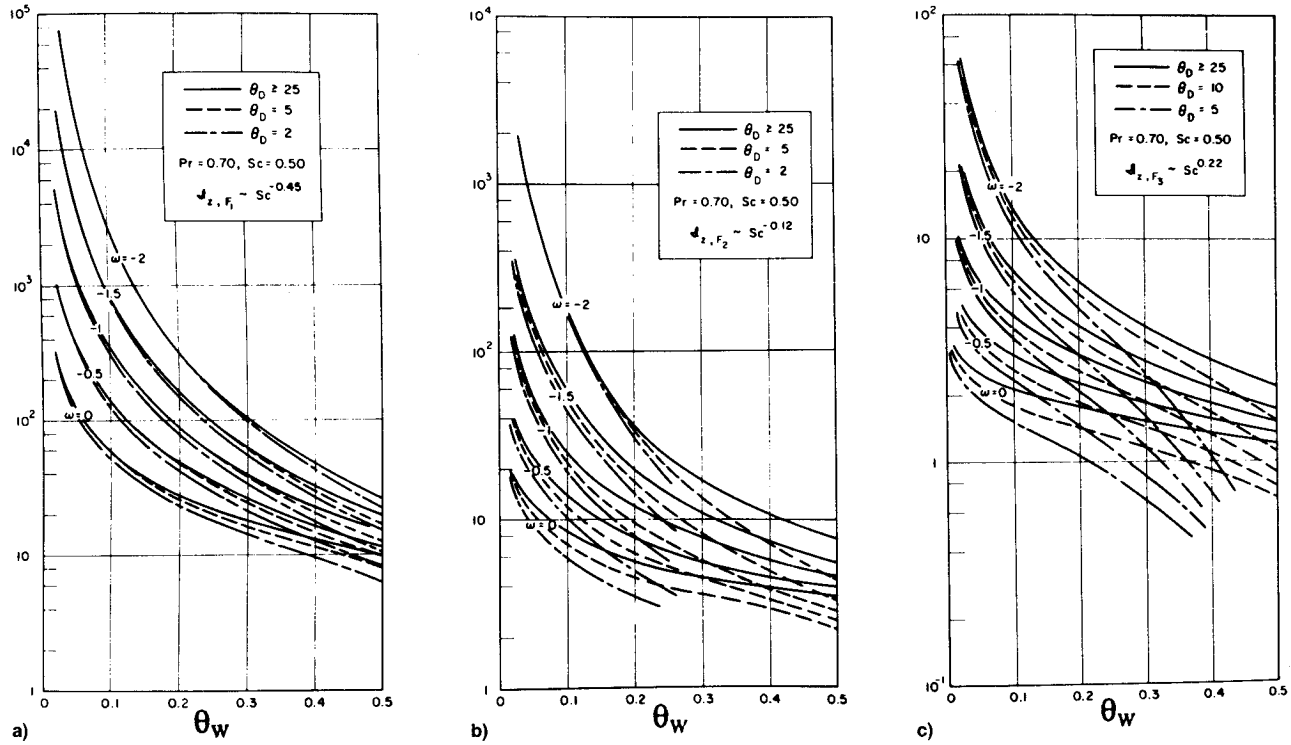

Fig. 3 Reaction rate integrals for recombination-dominated stagnation boundary layers: a) $\vartheta_{ZF,1}$, b) $\vartheta_{ZF,2}$, and c) $\vartheta_{ZF,3}$.

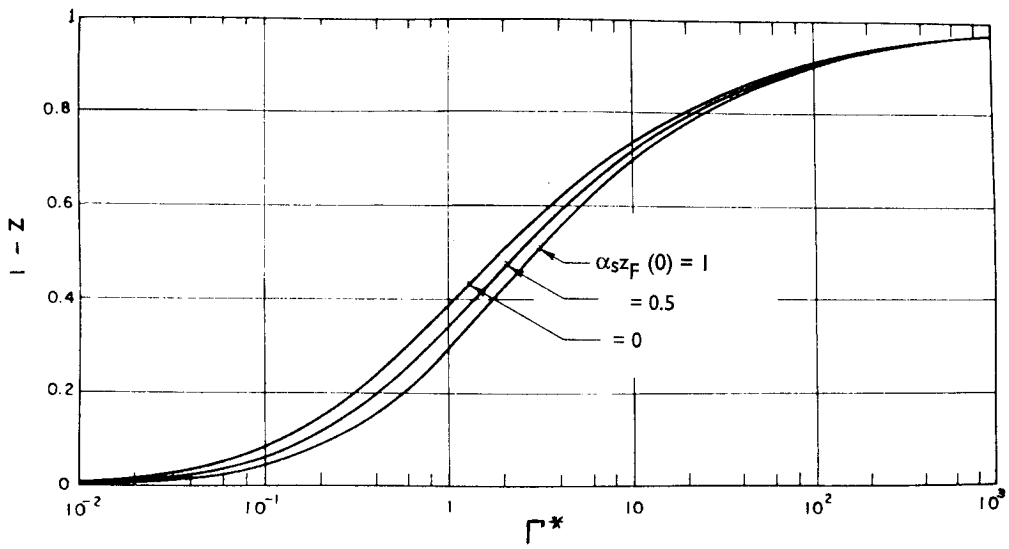

Fig. 4 Universal nonequilibrium boundary-layer solution for an arbitrarily catalytic stagnation point.

and (22), but it is emphasized that purely numerical values from any appropriate aerodynamic heating code would serve equally well. With the above as a basis, parametric studies have been made to illustrate this sensitivity to various important physical properties related to the vehicle size, the flight corridor conditions, and the chemical rate data. In carrying this out, the stagnation point velocity gradient β_s was evaluated from the relationship[6]

$$\beta_s \approx R_x^{-1}\sqrt{2(p_s - p_\infty)/\rho_\infty} \tag{24}$$

and the equilibrium dissociated-air properties behind the (normal) bow shock were obtained from Ref. 10. An example is shown in Fig. 7 for the sensitivity to the gas-phase recombination rate temperature-dependence exponent. Noting from Eq. (8) that the relative net reaction rate per unit density in the highly cooled boundary-layer region near the wall is proportional to θ_w^ω (with $\omega \cong -1.5$), we see for $\theta_w << 1$ that increasing ω toward positive values reduces gas-phase atom recombination in this region, and so drives the heat transfer toward the frozen value pertaining to the prevailing level of surface catalysis. Such results bring out the value of the present theory in assessing acceptable rate data accuracy for any desired engineering accuracy of nonequilibrium heat transfer prediction. Additional parametric study results can be found in Ref. 11.

Swept-Wing Leading-Edge Region

Owing to the sweepback angle involved, this region (Fig. 8) contains an attachment line type of flow with a significant spanwise component. The boundary-layer flow is again self-similar ($\partial/\partial\xi \equiv 0$) with $r = 0$ and $u_e^2/2\hat{C}_p T_e$ negligible; however, the spanwise kinetic energy parameter $w_e^2 = U_\infty^2 \sin^2\Lambda$ is significant for moderate-to-large sweep angles at hypersonic flight

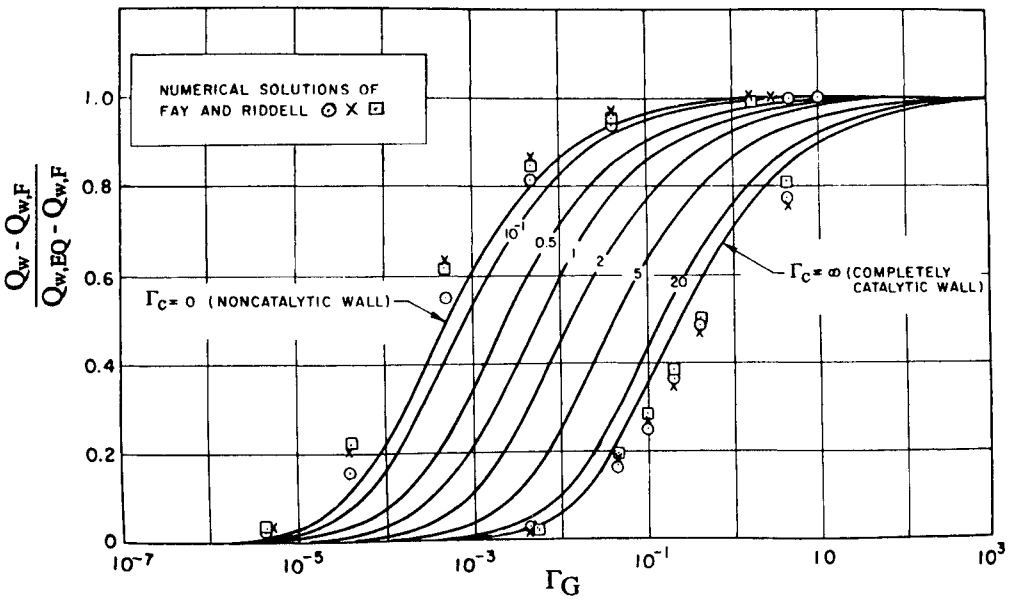

Fig. 5 Comparison of approximate analytical solution for nonequilibrium stagnation heat transfer vs exact numerical results ($\theta_w = 0.04$, $Sc = 0.5$, $Pr = 0.7$, $\omega = -1.5$, $\theta_D = 10$, $\alpha_s = 0.536$).

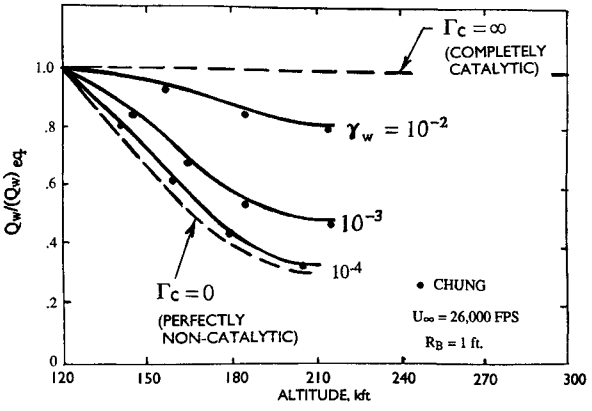

Fig. 6 Predicted nonequilibrium heat transfer variation with altitude for various surface catalytic efficiencies.

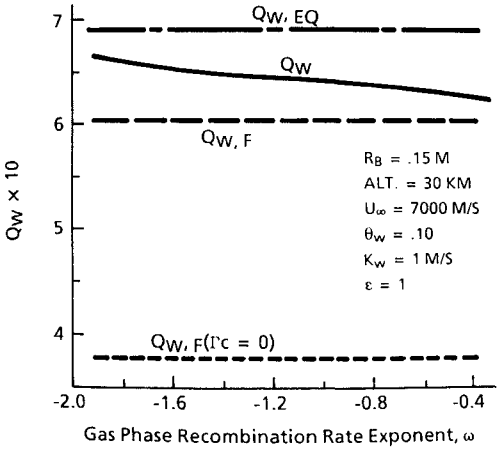

Fig. 7 Sensitivity of nonequilibrium heat transfer to gas-phase recombination rate temperature exponent ω ($k_r = k_r' T^\omega$).

speeds. The resulting formulation from Eqs. (1–10) constitutes a generalization of Fay and Riddell's well-known nonequilibrium stagnation point analysis[9] to embrace arbitrary surface catalycity and the effects of sweepback. This has been solved by means of a standard finite difference method[12] over many values of the various thermochemical parameters and both gas-phase and surface catalysis Dähmkohler numbers, for sweep angles ranging from 0 to 80 deg. The results obtained in the zero-sweep case were in excellent agreement with Fay and Riddell's predictions of both wall atom concentration and heat transfer throughout the entire nonequilibrium regime for either a fully catalytic or completely catalytic wall.

In relation to aerothermochemistry, sweepback can influence the nonequilibrium flow in three major ways. First, sweep significantly alters the equilibrium-dissociated inviscid flow at the edge of the boundary layer. As shown by the thermodynamic and energy relations that govern this (see Appendix), sweep rapidly reduces both the dissociation level $\alpha_e = \alpha_s$ and (especially) the static temperature T_s, along with the usual $\cos^2\Lambda$ reduction in static pressure: see Fig. 9. Such reductions tend to suppress both the recombination and dissociation rates in the gas phase. Second, sweepback alters the magnitudes of the basic Dähmkohler numbers Γ_G and Γ_c that control the relative degree of nonequilibrium in the gas phase and surface catalysis reactions, respectively. This is due to the combined effects on the inviscid gas state and on the chordwise stagnation velocity gradient that is proportional to cos Λ (Ref. 13). Considering the gas phase reaction parameter, we find for $\omega = -1.5$ that

$$\frac{\Gamma_G}{(\Gamma_G)_{\Lambda=0}} \cong \frac{T_s^\omega/\beta_s}{(T_e^\omega/\beta_s)_{\Lambda=0}} \cong (\cos\Lambda)^{2\omega-1} \cong \sec^4\Lambda \qquad (25)$$

since $p_s/p_{s0} = \cos^2\Lambda$, $T_s/T_{s_0} \leq \cos^2\Lambda$. At $\Lambda = 60$ deg, e.g., this predicts an order of magnitude increase, indicating that the crossflow drives the gas-phase reactions in the boundary layer toward equilibrium when recombination is dominant. Turning to the surface recombination parameter Γ_c, a similar type of analysis for a fixed wall temperature shows that

$$\Gamma_c/(\Gamma_c)_{\Lambda=0} = \cos^{1/2}\Lambda \qquad (26)$$

implying that sweep slightly reduces the effective catalycity of the wall. Third, the viscous dissipation heating associated with the spanwise boundary layer [i.e., the term $\sim w_e^2$ in Eq. (6)] can significantly affect the gas-phase reaction rate within the boundary layer, especially the dissociation rate. Consider

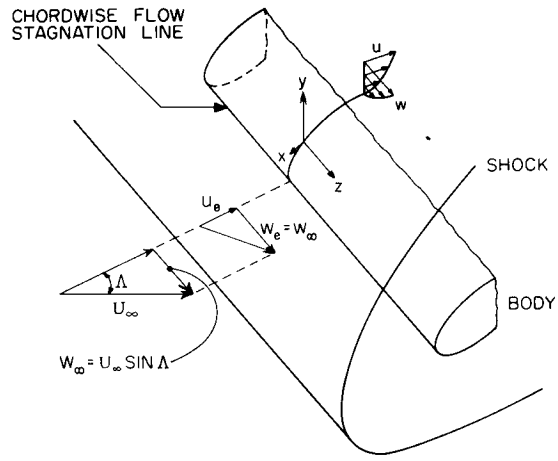

Fig. 8 Swept-wing leading-edge region: a reattachment line with sweep-induced crossflow.

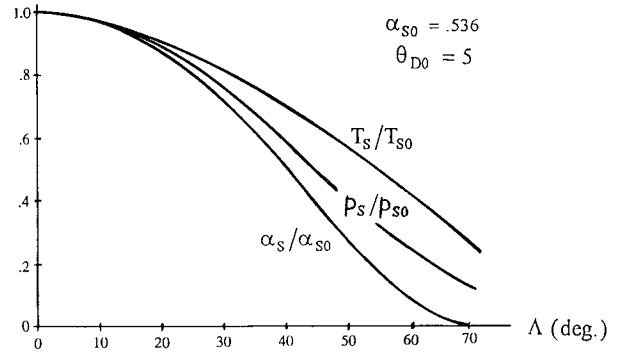

Fig. 9 Typical sweepback effects on inviscid equilibrium properties.

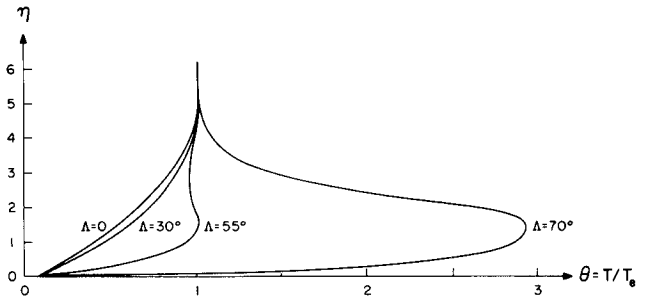

Fig. 10 Sweepback effect on boundary-layer temperature profiles.

Fig. 10, where typical boundary-layer temperature profiles are illustrated for various sweep angles. When the sweep angle is small to moderate and the crossflow dissipation heating thus small, the temperature drops monotonically inward across the boundary layer and the nonequilibrium gas-phase reaction is dominated by recombination ($\sim\theta^{\omega-2}\alpha^2$) near the cold surface. On the other hand, at large sweep angles $\Lambda > 60$ deg the crossflow dissipation causes a pronounced temperature overshoot and this can significantly affect the dissociation rate in the vicinity of this temperature maximum because of its exponential dependence ($\sim e^{-\theta_D/\theta}$).

Guided by the foregoing remarks, we now present typical results for the predicted sweepback effect on the nonequilibrium boundary-layer properties of wall atom concentration and heat transfer. To fix ideas, we have chosen for study the same zero sweep "baseline" case that was employed in Fay and Riddell's work: $\alpha_{S0} = 0.536$, $\theta_{D_0} = 5.0$, $\theta_{w0} = 0.04$. The first set of results deals with the influence of finite surface catalysis only, for the limiting case of chemically frozen gas-phase reaction ($\Gamma_G = 0$); these extend Goulard's well-known study of this limit[3] to include the influence of arbitrary sweep. Figure 11 shows the predicted sweepback effect on the wall atom concentration α_w for several values of Γ_{C_0} ranging from completely noncatalytic ($\Gamma_{C_0} = 0$) to fully catalytic ($\Gamma_{C_0} >> 1$). It is seen that the influence of sweep in reducing the Dähmkohler number is rather small, causing only a slight increase in α_w when Γ_{C_0} is of order unity. Far more significant is the influence of the reduction in α_s with sweep, which correspondingly reduces α_w such that it vanishes for sweep angles above 60 deg. The same trend is also reflected in the corresponding sweepback effect on heat transfer, as shown in Fig. 12 [note here that we have plotted $\dot{q}_w$, which reflects the additional sweep effects on $\hat{C}_p T_s$ and $\rho_w \mu_w \beta_s \sim \cos^{3/2}$ multiplied through from the denominator of Eq. (10)]. The overall aerothermochemical effect of sweep is clearly seen: it wipes out the dissociation effects altogether beyond $\Lambda = 60$ deg, such that the considerable beneficial effect of a noncatalytic wall in reducing zero sweep heat transfer is completely eliminated, leaving only the usual ideal gas sweep-reduction effect proportional to $\sim(\hat{C}_p T_s/\hat{C}_{p_0} T_{s_0})\cos^{3/2}\Lambda$.

Turning to the gas-phase chemistry aspects of the flow, some cases of α_w vs Λ on a noncatalytic wall for various values Γ_{G_0} are plotted in Fig. 13 so as to show the individual contributions of the various factors described above. It is seen that notwithstanding the significant spanwise viscous dissipation heating effect on the reaction rates (especially dissociation), which alone tends to increase α_w significantly with sweep, the counterbalancing effects from the reduction in α_s and T_s (especially the attendant rise in $\theta_D \sim T_s^{-1}$) are even stronger with the net result that sweep diminishes the gas-phase dissociation effect to virtually zero beyond $\Lambda = 60$ deg. Qualitatively, the role of sweep is thus the same as found above for catalytic surface reaction. The corresponding non-

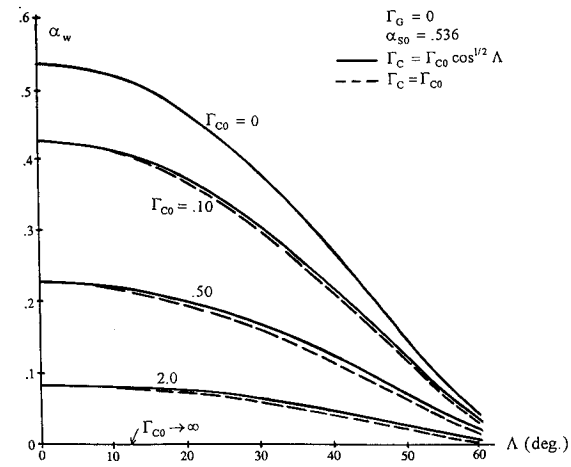

Fig. 11 Sweepback effect on wall atom concentration for frozen gas-phase flow.

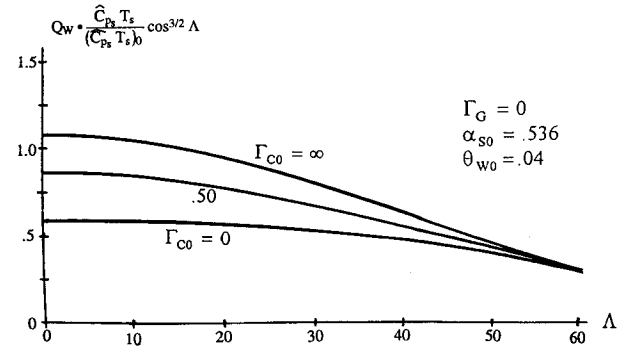

Fig. 12 Sweepback effect on heat transfer in frozen flow.

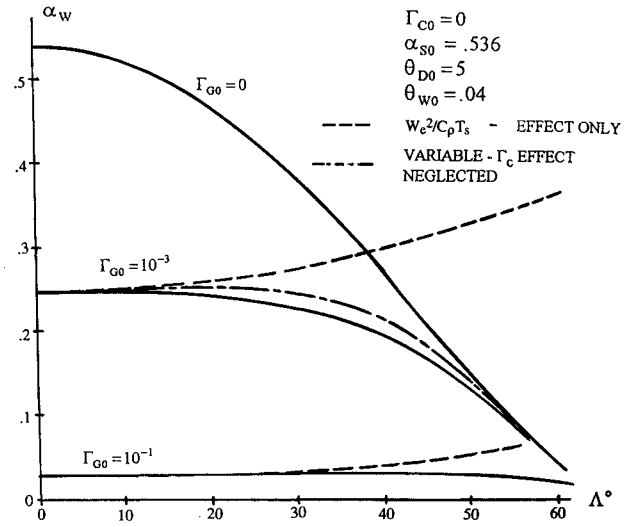

Fig. 13 Sweepback effect on nonequilibrium atom concentration at a noncatalytic wall.

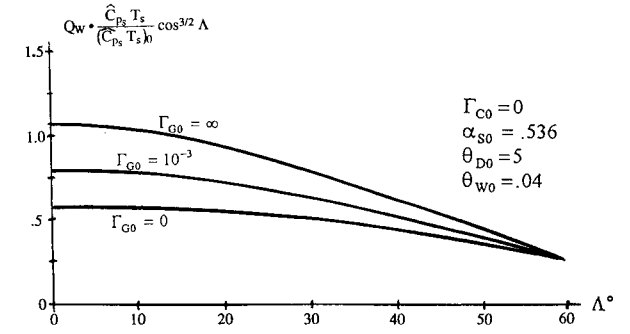

Fig. 14 Sweepback effect on nonequilibrium heat transfer to a noncatalytic wall.

equilibrium heat transfer variations with sweep are presented in Fig. 14 and mirror the same conclusions.

Windward Centerline Region

Since the inviscid equilibrium flow along this surface streamline is approximately isobaric downstream of the nose, the underlying laminar boundary-layer flow without finite rate chemistry would necessarily follow local flat plate similarity behavior. When nonequilibrium dissociation–recombination is present within the boundary layer and/or finite catalytic surface, atom recombination occurs, however, the corresponding viscous thermochemistry is no longer strictly self-similar along the windward centerline and this should be taken into account to obtain the most accurate local nonequilibrium flow property predictions (although the local similarity approximation would probably be sufficiently accurate for engineering heat transfer calculations[5]). Taking this flow to be laterally symmetric, we have $\Lambda = r = 0$ and approximately constant pressure p_e and inviscid velocity u_e downstream of the nose. Moreover, for slender bodies at small angles of attack, hypersonic small disturbance theory[6] shows that u_e is approximately equal to the flight speed U_∞. At hypersonic flight speeds, this results in large values of the local viscous dissipation heating term ($\sim u_e^2/2\hat{C}_pT_e$) in the temperature profile [Eq. (6)] and, hence, a net nonequilibrium reaction rate that is dominated by the exponential dissociation contribution.

A revealing and useful analytical treatment of this dissociation rate-dominated nonequilibrium flow region can be obtained by exploiting its exponential temperature dependence and sharp peak around the maximum $\theta^*(\eta^*)$. Thus, by applying LaPlaces method,[14] the reaction function $\mathcal{R}$ can be approximated well by[15]

$$\mathcal{R} = \mathcal{R}^* \exp\left[\frac{\theta_D(\eta - \eta^*)^2|\theta''(\eta^*)|}{2\theta^{*2}}\right] \tag{27}$$

where $\mathcal{R}^* = \mathcal{R}(\eta^*)$ is the maximum reaction rate and θ'' is found by direct differentiation of Eq. (6). Furthermore, when the boundary layer is well out of equilibrium we may further evaluate Eq. (27) on the basis of the frozen-flow temperature function

$$\theta_F''(\eta^*) \cong -\sqrt{Pr}(U_\infty^2/\hat{C}_pT_e)[f''(\eta^*)]^2 \tag{28}$$

where η^* is located within the boundary layer by the condition $f'(\eta^*) \cong 1/2$ pertaining to hypersonic cold wall flows. Then integration of species Eq. (5) in a manner similar to Eqs. (12–16) yields the following expression governing the atom concentration along an arbitrarily catalytic wall (see Ref. 15 for details):

$$\alpha_w = \alpha_{w,F} + \frac{\Gamma_D \vartheta_D}{1 + \Gamma_c I_z(\infty)} \tag{29}$$

where Γ_D is a new dissociation Dähmkohler number

$$\Gamma_D \equiv \frac{4C_D k_r' T_e^{\omega-2}}{\mathcal{R}_u^2 u_e} \cdot p_e x \tag{30}$$

and the dissociation-rate integral $\vartheta_D = \vartheta_z(\infty)$ of Eq. (16) takes the form

$$\vartheta_D \cong -F^* \cdot G(\alpha_F^*, \theta_F^*) \tag{31}$$

involving the product of the local maximum reaction rate and a form factor F^* that accounts for the integrated effect of diffusion and convection on the reaction rate distribution across the boundary layer (see Refs. 14 and 15). Typical numerical values of this integral as functions of θ_D, θ_w, and the parameter $\mathcal{U} \equiv U_\infty^2/2\hat{C}_pT_e$ are presented in Fig. 15, where it can be seen that they are virtually independent of the surface catalycity in this dissociation-dominated regime where θ_D and $\mathcal{U}$ are both large.

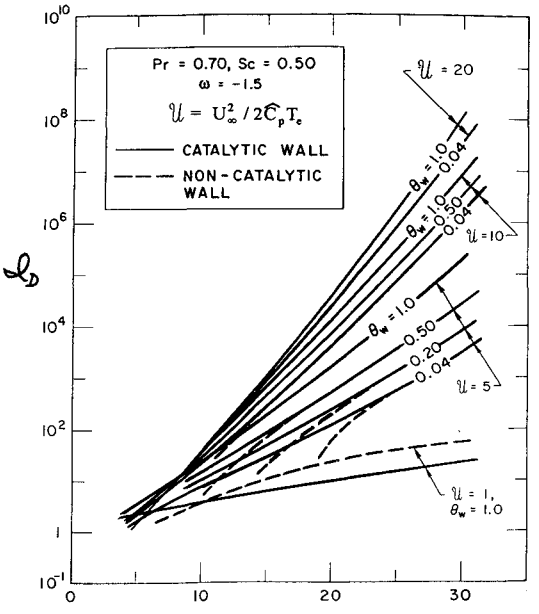

Fig. 15 Reaction rate integrals for dissociation-dominated nonequilibrium boundary-layer flow along the windward centerline.

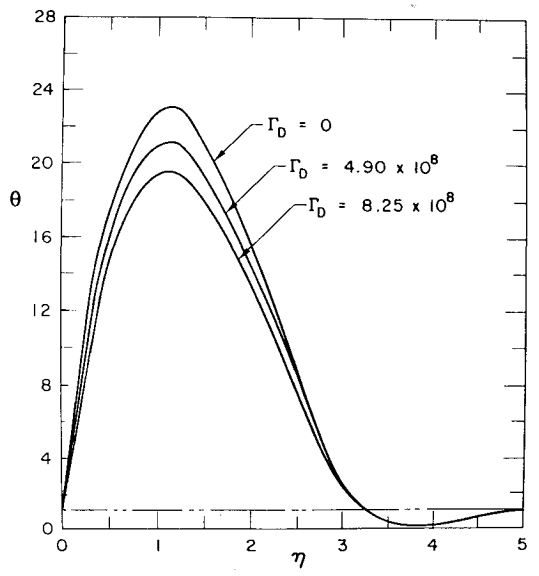

Fig. 16 Boundary-layer temperature profiles along the downstream dissociation-dominated flow region (Sc = 0.5, Pr = 0.7, $T_w = T_e$ = 253 K, $\omega = -1.5$).

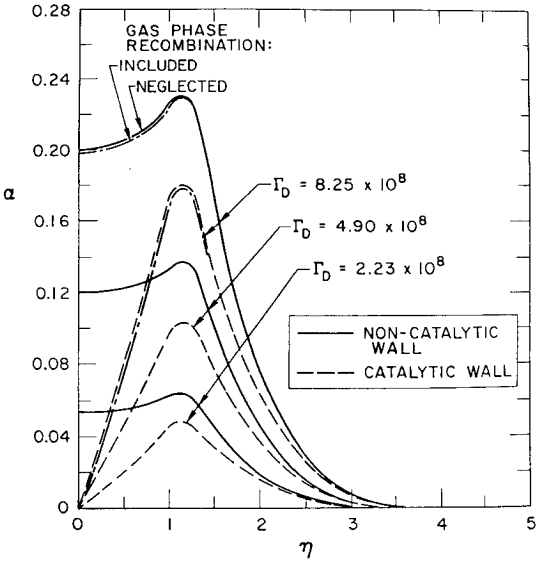

Fig. 17 Boundary-layer atom concentration profiles along the downstream dissociation-dominated flow (Sc = 0.5, Pr = 0.7, $T_w = T_e$ = 253 K, $\omega = -1.5$).

Equation (29) predicts that on a wall of low-to-moderate catalycity $0 \leq \Gamma_c \leq 0(1)$, the dissociation-dominated nonequilibrium chemistry increases the atom concentration on the wall. When the wall is highly catalytic such that $\Gamma_c >> \Gamma_D \cdot \vartheta_D$ and $\alpha_F(0) = 0$, however, α_w is virtually zero regardless of the gas-phase chemistry as indeed one would expect. Typical atom and temperature profile solutions pertaining to this solution are illustrated in Figs. 16 and 17 for both noncatalytic and catalytic wall cases; the downstream growth of the atom concentration level due to nonequilibrium dissociation predicted by Eq. (29) is evident from these curves. It should be noted that these solutions also possess a property of binary scaling,[16] since with recombination neglected Eq. (30) indicates that the nonequilibrium effects depend only on the product $p_e x$ for a given flight velocity, type of gas, and wall temperature.

The corresponding heat transfer is obtained from Eqs. (6), (10), and (29) as

$$Q_w \approx Q_{w,F} - \Delta Q \cdot \Gamma_D \vartheta_D \tag{32a}$$

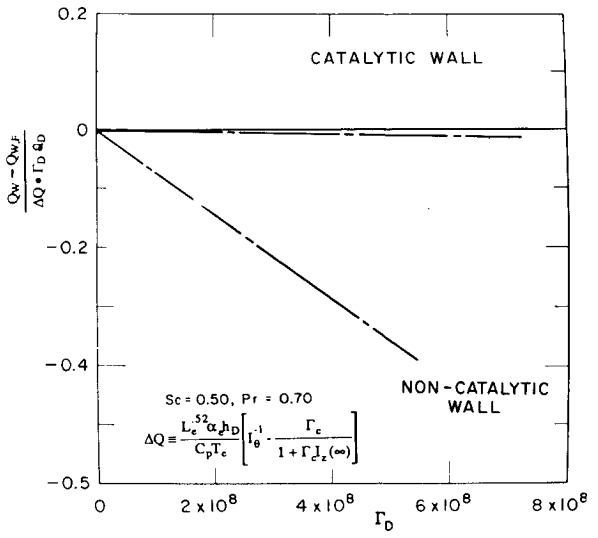

Fig. 18 Variation of heat transfer with dissociation Dähmkohler number along the windward centerline.

where

$$\Delta Q \equiv \frac{h_D}{I_\theta \hat{C}_p T_e}\left[1 - \left(\frac{Le\tilde{\Gamma}_c}{1 + \tilde{\Gamma}_c}\right)\right] \tag{32b}$$

is a nondimensional nonequilibrium heat transfer increment that depends on the surface catalycity. As illustrated in Fig. 18, Eq. (32) predicts that the dissociation-dominated nonequilibrium effect significantly reduces the heat transfer except in the highly catalytic case where ΔQ is so small that the second nonequilibrium term on the right side of Eq. (32a) is negligible compared to $Q_{w,F}$. The accuracy of the foregoing analysis has been checked for dissipation heating-dominated hypersonic boundary layers along a flat plate with analogous dissociation-controlled nonequilibrium physics: the theory gave results within 5% of exact numerical solutions over a wide range of flight conditions, except very close to the equilibrium state.[14]

Concluding Remarks

The present investigation has shown that some appropriate simplifying approximations pertaining to the boundary-layer chemistry on highly cooled vehicles can be exploited to develop useful analyses of the nonequilibrium heat transfer in each of three critical heating regions on arbitrarily catalytic surfaces. These enable cost-effective engineering design studies and improve the physical insight into the processes in the boundary layer that govern diffusion, gas-phase reaction, and surface recombination. Moreover, the developed solutions prove useful in interpreting purely numerical viscous codes that deal with nonequilibrium flows.

A desirable extension of this work would be the inclusion of further nonequilibrium effects in the inviscid flow as encountered at very high altitude (low Reynolds number) flight conditions above roughly 250,000 ft altitude where the boundary layer has thickened to occupy a significant portion of the shock layer.

Appendix: Sweep Effects on Inviscid Dissociated Flow

We suppose that the inviscid equilibrium values of stagnation pressure, temperature, and degree of dissociation for zero sweep (p_{s0}, T_{s0}, α_{s0}, respectively), are known for each desired altitude and flight speed as obtained from a standard normal shock table.[10] Then the relative effects of sweep on these values can be determined as follows for hypersonic speeds where the freestream ambient energy $\hat{C}_{p\infty} T_\infty << U_\infty^2/2$.

The steady flow energy equation required that $\hat{C}_{p_s} T_s = \frac{1}{2} U_\infty^2 \cos^2\Lambda / [1 + (\alpha_{s_0} R_M / \hat{C}_{p_0}) \theta_{D_0}]$, which in turn implies the ratio

$$\frac{\hat{C}_{p_s} T_s}{\hat{C}_{p_0} T_{s_0}} = \left(1 + \frac{\alpha_{s_0} R_M}{\hat{C}_{p_0}} \theta_{D_0}\right) \cos^2\Lambda - \frac{\alpha_s R_M}{\hat{C}_{p_0}} \theta_{D_0} \quad \text{(A1)}$$

Using the value of the dissociated gas mixture specific heat that $\hat{C}_p / R_M \cong 7(1 - \alpha_s)/2 + 5\alpha_s$, we further have that

$$\frac{\hat{C}_{p_s}}{\hat{C}_{p_0}} \cong \frac{7 + 3\alpha_s}{7 + 3\alpha_{s_0}} \quad \text{(A2)}$$

Finally, from the equilibrium dissociation relationship (law of mass action) in which we take $C_D = p_{s_0} \alpha_{s_0}^2 e^{\theta_{D_0}} / (1 - \alpha_{s_0}^2)$ there is obtained the equation governing α_s that

$$\frac{\alpha^2}{1 - \alpha_s^2} = \left(\frac{\alpha_{s_0}^2}{1 - \alpha_{s_0}^2}\right) \sec^2\Lambda e^{\theta_{D_0} - \theta_D} \quad \text{(A3)}$$

where we have used $p_s / p_{s_0} \cong \cos^2\Lambda$, and where it is noted that $\theta_D = T_{s_0} \theta_{D_0} / T_s$. A simultaneous solution of Eqs. (A1–A3) for $\Lambda > 0$ then yields the sweep effect on $\hat{C}_p$, T_s, α_s, and then θ_D for a given set of the unswept parameters.

With the foregoing in hand, the crossflow viscous dissipation heating parameter can then be determined using $w_e^2 = U_\infty^2 \sin^2\Lambda$ as

$$\frac{w_e^2}{2\hat{C}_p T_s} = \frac{U_\infty^2 \sin^2\Lambda}{2\hat{C}_p T_s} = \left(1 + \frac{\alpha_s h_D}{C_p T_s}\right) \tan^2\Lambda \quad \text{(A4)}$$

with $h_D / \hat{C}_p T_s = 2\theta_D / (7 + 3\alpha_s)$.

References

[1]Anderson, J. D., Lewis, M., and Kothedi, A., "Hypersonic Waveriders for Planetary Atmospheres," AIAA Paper 90-0538, Jan. 1990.

[2]Shindell, L. H., "Waveriders," *Tactical Missile Aerodynamics*, Vol. 24, Progress in Astronautics and Aeronautics, AIAA, Washington, DC, 1988, pp. 198–242.

[3]Goulard, R. J., "On Catalytic Recombination Rates in Hypersonic Stagnation Heat Transfer," *Jet Propulsion,* Vol. 28, No. 11, 1958, pp. 737–745.

[4]Chung, P. M., "Hypersonic Viscous Shock Layer of Nonequilibrium Dissociating Gas," NASA Rept. R-109, May 1961.

[5]Lees, L., "Laminar Heat Transfer over Blunt-Nosed Bodies at Hypersonic Flight Speeds," *Jet Propulsion*, Vol. 26, No. 4, 1956, pp. 259–268.

[6]Hayes, W. D., and Probstein, R. F., *Hypersonic Flow Theory*, Academic, New York, 1959, pp. 293–312.

[7]Reshotko, E., "Heat Transfer to a General Three-Dimensional Stagnation Point," *Jet Propulsion*, Vol. 28, No. 1, 1958, pp. 58–60.

[8]Inger, G. R., "Nonequilibrium Stagnation Point Boundary Layers with Arbitrary Surface Catalycity," *AIAA Journal*, Vol. 1, No. 8, 1963, pp. 1776–1784.

[9]Fay, J. A., and Riddell, F. R., "Theory of Stagnation Point Heat Transfer in Dissociated Air," *Journal of Aeronautical Sciences*, Vol. 25, No. 2, 1958, pp. 73–85.

[10]Wittliff, C. E., and Curtis, J. T., "Normal Shock Wave Parameters in Equilibrium Air," Cornell Aeronautical Labs, Rept. CAL-111, Buffalo, NY, June 1961.

[11]Inger, G. R., and Elder, J., "Recombination Dominated Nonequilibrium Heat Transfer to Arbitrarily-Catalytic Hypersonic Vehicles," *Journal of Thermophysics and Heat Transfer*, Vol. 5, No. 4, 1992, pp. 449–455.

[12]Moran, J., *An Introduction to Theoretical and Computational Aerodynamics*, Wiley, New York, 1984, pp. 289–295.

[13]Reshotko, E., and Beckwith, I. E., "Compressible Laminar Boundary Layer over a Yawed Infinite Cylinder with Heat Transfer and Arbitrary Prandtl Number," NACA Rept. R-1379, June 1957.

[14]Rae, W. J., "A Solution for the Nonequilibrium Flat-Plate Boundary Layer," *AIAA Journal*, Vol. 1, No. 6, 1963, pp. 2279–2286.

[15]Inger, G. R., "Highly-Nonequilibrium Boundary Layer Flows of a Multi-Component Dissociated Gas Mixture," *International Journal of Heat and Mass Transfer*, Vol. 7, No. 11, 1964, pp. 1151–1174.

[16]Gibson, W. E., "Dissociation Scaling for Nonequilibrium Blunt Nose Flows," *Journal of the American Rocket Society*, Vol. 32, No. 2, 1962, pp. 285–287.